A Thermocouple Probe for High-Speed Temperature Measurement in the Ocean

JONATHAN D. NASH, DOUGLAS R. CALDWELL, MICHAEL J. ZELMAN, AND JAMES N. MOUM

College of Oceanic and Atmospheric Sciences, Oregon State University, Corvallis, Oregon

(Manuscript received 18 August 1997, in final form 9 November 1998)

ABSTRACT

A fast-response chromel–constantan thermocouple sensor was constructed for use on the microstructure profiler Chameleon and used for 60 ocean profiles off the coast of Oregon. The stability of the thermocouple was compared to that of an FP07 microbead thermistor, and its frequency response was compared to a high-resolution microconductivity probe. Although noisier than the thermistor, the thermocouple was found to be stable, to resolve temperature gradients at least 10 times thinner than the thermistor, and to be sufficiently robust for routine oceanic use.

1. Introduction

a. Motivation

The Osborn–Cox calculation (Osborn and Cox 1972) of turbulent heat flux requires an estimate of the rate of dissipation of temperature variance, χ_T, which may be approximated using vertical gradients as

$$\chi_T = 6D_T\left\langle\left(\frac{\partial T}{\partial z}\right)^2\right\rangle = 6D_T\int_0^\infty \Psi_{T_z}(k)\,dk, \qquad (1)$$

where k is the vertical wavenumber and D_T is the thermal diffusivity. To make an accurate estimate of χ_T, the temperature-gradient spectrum $\Psi_{T_z}(k)$ must be resolved to the smallest scale on which it varies, the Batchelor scale, $k_b^{-1} = (\nu D_T^2/\epsilon)^{1/4}$, where ν is the kinematic viscosity and ϵ is the rate of viscous dissipation of turbulent kinetic energy (Batchelor 1959; Caldwell et al. 1980; Oakey 1982).

At typical drop speeds for tethered profilers (~1 m s^{-1}), the commonly used thermistor temperature sensors do not resolve the entire temperature spectrum. It has become customary to estimate χ_T by applying large corrections to the unresolved thermistor signal, assuming the Batchelor (1959) form[1] for temperature-gradient spectrum (Gregg and Meagher 1980). The level of the Batchelor spectrum is determined from the low-wavenumber thermistor signal; then the shear probe estimate of ϵ (and hence k_b) is used to determine the high-wavenumber extent of the spectrum. Typically only 2%–50% of the variance of dT/dz is measured directly; most of the estimate of χ_T comes from the extrapolation. Figure 1 shows how the wavenumber resolution of a temperature sensor affects the fraction of Ψ_{T_z} resolved for various values of ϵ.

Error can easily be introduced through such large corrections. For example, the value of q (the parameter relating ϵ to the least principal strain rate γ) in the Batchelor spectrum is unknown; estimates range from $q = 2$ (Batchelor 1959) to $q = 12$ (Gargett 1985). The value chosen for q affects the estimate of χ_T dramatically. It is also possible that q might not be constant but rather a function of ϵ or the age of a patch. More important, the Batchelor spectral shape might be inappropriate. It is hence paramount to resolve as much of the turbulent temperature-gradient spectrum as possible to estimate χ_T. In the future we will address these issues as research topics; for now the Batchelor spectrum is used only as an indication of typical spectra in the ocean.

Uncertainties also arise because the spectral response of each thermistor is unique to that sensor (Lueck et al. 1977) and the profiling speed. Since it is too costly to determine the frequency response correction for each thermistor individually, a single formula is generally used, thereby introducing errors (Gregg 1997). Further, any error in estimating k_b from shear probes produces an error in χ_T.

b. Sensor requirements

To measure 80% of the temperature-gradient variance in an energetic turbulent patch ($\epsilon = 1 \times 10^{-6}$ m^2 s^{-3}),

[1] Although not universally accepted as a form for turbulent scalar spectra, we use the Batchelor form as a benchmark. An alternate form has been proposed by Kraichnan (1968).

Corresponding author address: Dr. Douglas R. Caldwell, College of Oceanic and Atmospheric Sciences, Oregon State University, 104 Ocean Admin. Bldg., Corvallis, OR 97331.
E-mail: caldwell@ccmail.orst.edu

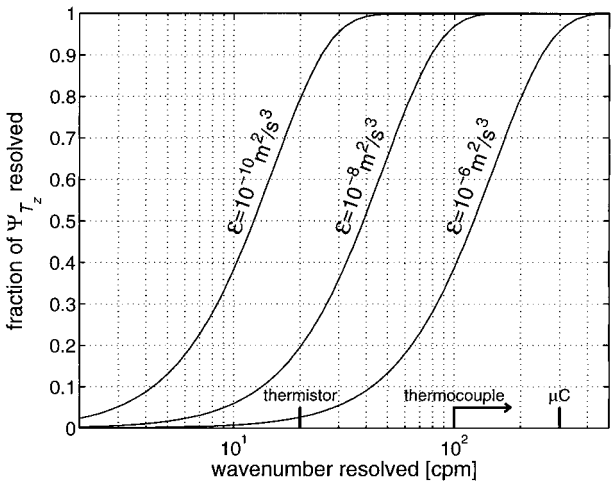

FIG. 1. The fraction of temperature-gradient spectrum resolved depends on ϵ and the highest wavenumber resolved by the sensor. For a profiling speed of 1 m s^{-1}, the resolved wavenumber for thermistor, thermocouple, and microconductivity probe are 20 cpm, better than 100 cpm, and 300 cpm, respectively.

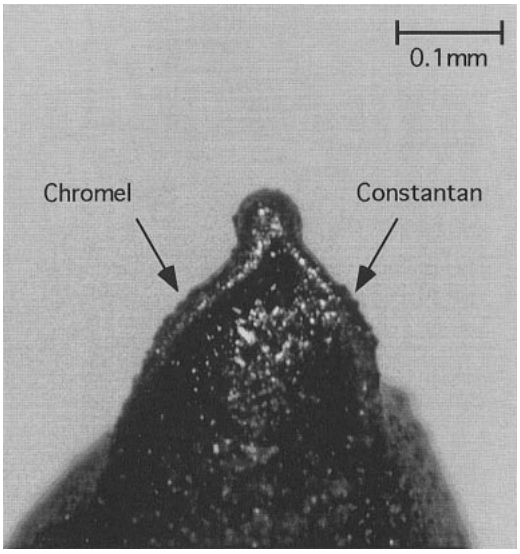

FIG. 2. Photograph of sensor junction.

a temperature sensor must resolve dT/dz from 0 to 200 cpm (Fig. 1). To do this from an instrument profiling at 1 m s^{-1}, fluctuations at frequencies of 200 Hz must be resolved. This corresponds to a sensor with single-pole time constant[2] less than $\tau = 0.8$ ms and spatial resolution better than 0.8 mm.

The common method of determining temperature gradient in the ocean uses a Thermometrics FP07 thermistor, which is smaller than 0.8 mm. However, the fluid boundary layer and coating surrounding the semiconductor bead limit heat transfer (Lueck et al. 1977), and response is attenuated 50% in power by 20 Hz. Small ''microconductivity'' probes can be used to sense temperature in regions where salinity gradients are negligible. These probes are small and fast enough. However, they do not work in freshwater and their signals include contributions from salinity variations in a complicated way (Washburn et al. 1996; Nash and Moum 1999). Cold-film sensors have been used (Oakey 1982), but their response is not as fast as desired, and are noisy, unstable, and fragile. Thermocouples have been used in the ocean (Urick and Searfoss 1948; Lieberman 1951; Marmorino and Caldwell 1978) but have not found general usage.

Thermocouples are routinely used as fast temperature sensors to study chemical reaction kinetics, mixing, and combustion (Balko and Berger 1968; Beckman et al. 1993; Fish et al. 1995). They are well suited to high-speed applications because they can be made as bead junctions as small as 30 μm in diameter. In contrast to thermistors, thermocouples do not need to be electrically (and hence thermally) insulated from the fluid. Such thermocouples are actually faster than required for our applications. They operate by the Seebeck effect, the principle that the electric potential produced at the junction between two dissimilar metals depends only on the nature of the two metals and the temperature of the junction.

Signal-to-noise ratio is a significant concern for thermocouple use in oceanic applications. For this reason, chromel–constantan junctions were chosen. They have the highest temperature sensitivity of the standard thermocouple metal pairs (6×10^{-5} V K^{-1}).

2. Probe construction

The probe tip consists of an exposed and uncoated 65-μm-diameter thermocouple bead (Omega Engineering Inc., part no. CHCO-001) supported by an epoxy matrix through which the 26-μm leads pass (Fig. 2). Each bare lead was soldered to insulated 30 gauge wire of the same metal type about 1 cm from the tip junction. This assembly was epoxied into a 6-mm-diameter, 15-cm-long stainless steel tube (Fig. 3), which fits into the nose of Chameleon, our microstructure profiler (Moum et al. 1995).

The wiring was continued with constantan wires on one lead and chromel on the other until reaching the cold junction compensator (Analog Devices AC1226), which measures the temperature of the reference junction inside Chameleon's pressure case. To reduce noise, the chromel–copper and constantan–copper junctions were made in close thermal contact to the compensator but are not electrically connected. If electrically con-

[2] The time constant is defined as the time required for a sensor to reach 1/e of its final value in response to a step change in temperature. If the response is similar to that of a single-pole filter, a device with time constant τ has a 50% response in power at a frequency $(2\pi\tau)^{-1}$ [Hz]. Similarly, a double-pole filter attenuates 75% of the power at the frequency $(2\pi\tau)^{-1}$.

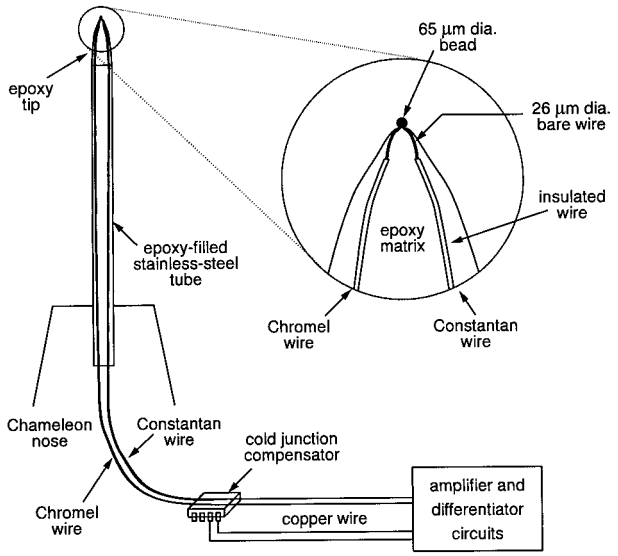

FIG. 3. Schematic representation of the probe and circuitry.

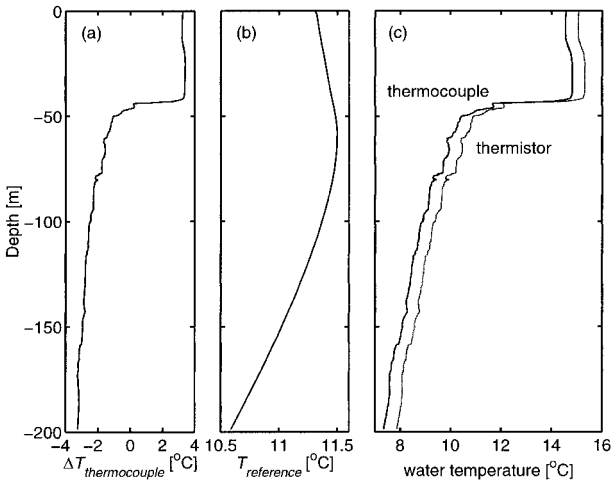

FIG. 4. Computation of the water temperature profile by combining thermocouple and cold-junction compensator signals. (a) The temperature difference between sensor tip and cold junction compensator is the signal measured by the thermocouple $\Delta T_{\text{thermocouple}}$. This temperature difference is added to the reference temperature $T_{\text{reference}}$ measured at (b) the cold junction to determine the (c) absolute water temperature. The thermistor-derived temperature profile (offset by 0.5°C) is shown in gray for comparison.

nected, the cold junction compensator introduces noise into the signal.

The thermocouple voltage was amplified by a factor of 8207 using an AD745 operational amplifier for the first stage (gain = 16) and AD797 and OP400 for the final stages. The signal was digitally sampled at 204.8 Hz and also differentiated and sampled 409.6 Hz. The output of the electrically isolated cold junction compensator signal was separately amplified and sampled at 102.4 Hz. Each signal was low-pass filtered prior to sampling to prevent aliasing.

3. Testing and evaluation

Thermocouple sensors were installed on Chameleon (Moum et al. 1995) along with a fast ''microconductivity'' probe,[3] two thermistors (one coincidently located with the microconductivity probe), a slow conductivity sensor, pressure sensor, shear probe, and accelerometers. We tested this package on two occasions in the ocean near the Oregon coast from R/V *Wecoma* and in freshwater at Green Peter Reservoir, Oregon. Results from 100 downward profiles in the ocean at ~0.3 m s^{-1} and ~1.2 m s^{-1} are used in the following evaluation.

As a benchmark temperature sensor for stability and noise, we use the Thermometrics FP07 fast-response thermistor. The thermistors were calibrated using a SeaBird temperature cell in our lab. The dynamic response of this type of thermistor has been documented by Lueck et al. (1977) and Gregg and Meagher (1980) but is revisited in the appendix. Because the response of the thermistor is highly attenuated at high frequencies, we use the microconductivity probe and conductivity gradient as a proxy for temperature gradient at high frequencies. The resolution of the microconductivity probe depends on the volume over which conductivity is measured; Head (1983) and Nash and Moum (1998) find that the power response is well described by a double-pole filter with 3-dB point at 300 cpm. In regions where the salinity gradient dS/dz is small, the temperature gradient can be estimated from the conductivity gradient dC/dz (Washburn et al. 1996) as

$$\frac{dT_{\mu C}}{dz} = \left(\frac{dC}{dz}\right)\left(\frac{\partial C}{\partial T}\right)_S^{-1}, \tag{2}$$

where $(\partial C/\partial T)_S$ represents the change in conductivity with temperature at constant salinity. We refer to the spectrum of $dT_{\mu C}/dz$ as $\Psi_{\mu C_z}$, which has the same units as Ψ_{T_z}, [K^2 m^{-2} Hz^{-1}].

a. Absolute temperature

1) COMPUTATION

The thermocouple measures the temperature difference between the sensor tip and Chameleon's internal temperature at the location where the chromel and constantan wires change to copper at the cold junction compensator. The water temperature is thus the sum of the cold junction compensator temperature $T_{\text{reference}}$ and the thermocouple temperature difference $\Delta T_{\text{thermocouple}}$ (Fig. 4).

The internal temperature $T_{\text{reference}}$ changes during a profile as a result of thermal transfer between the in-

[3] The microconductivity probe is manufactured by M. Head of Precision Measurement Engineering and is described by Head (1983) and Nash and Moum (1998).

strument and the surrounding water. Above the thermocline, $T_{\text{reference}}$ increases as heat flows from the warm surface waters to the cold instrument body, which has just been at depth during the previous profile. Below the thermocline, the instrument cools but remains above the temperature of the surrounding water because of heat produced by Chameleon's electronics.

2) SOURCES OF ERROR

The Seebeck voltage referenced to 0°C of the chromel–constantan pair is weakly nonlinear, and for $0°C < T < 25°C$ is approximately [from table Z-170 in Omega Engineering (1995)]

$$V = 58.7(T + 0.000\,78T^2), \tag{3}$$

with T in degrees Celsius and V in microvolts. This gives a sensitivity of 59.6 μV K^{-1} at 10°C. We find that the sensitivity of individual thermocouples varies and at 10°C is 57.5–58.6 μV K^{-1} for our probes, which is slightly less than the published value.

Imperfect thermal contact between the cold junction compensator and the reference junctions can lead to error in the computed temperature. Since $T_{\text{reference}}$ is not maintained constant, heat must flow into and out of the compensator. The temperature of the reference junctions (located directly on top of the compensator chip) will thus be slightly less or more than $T_{\text{reference}}$, depending on whether the instrument is warming or cooling. This effect introduces a small systematic error in the computed temperature.

Error is also introduced in the measurement of $T_{\text{reference}}$ by the cold junction compensator (AC1226), which we find to be noisy. Its signal is contaminated by a 5-mK sawtooth wave at 3 Hz and other broadband noise. Hence, $T_{\text{reference}}$ was low-pass filtered at 0.5 Hz before combining it with $\Delta T_{\text{thermocouple}}$; higher frequency variation of the reference junction temperature is not expected. Furthermore, during our week of testing, we experienced a discrete change in offset voltage between one set of profiles and three other sets of profiles. This offset produced a 0.5-K change in computed water temperature, which we attribute to the AC1226, which claimed to have an absolute accuracy of 0.5 K.

We have since discarded the AC1226 and use a National Semiconductor LM35CA precision centigrade temperature sensor to measure $T_{\text{reference}}$. We find this sensor to be much more stable and have used it for 800 profiles during the summer of 1998, achieving an absolute accuracy of 0.1 K.

The rms deviation between the thermocouple and either of Chameleon's two thermistors is about 10 mK once the thermocouple sensitivity and compensator offset are determined. In comparison, the rms deviation between the pair of FP07 thermistors is about 5 mK. One reason for these differences is that the probes are spaced 4 cm apart and are measuring slightly different events. Another reason is that the thermocouple responds faster and is measuring variance at higher frequencies than the thermistors can resolve.

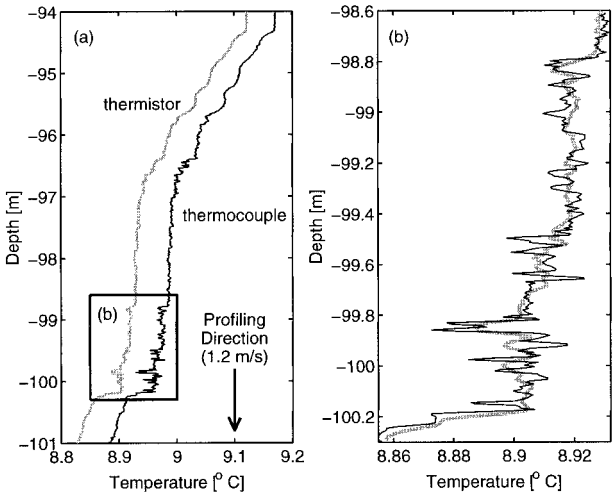

FIG. 5. Vertical profiles of temperature as measured by the thermistor (thick gray line) and thermocouple [thin black line, offset by 0.05°C in (a)] while profiling downward at 1.2 m s^{-1}. The expanded view of the turbulent patch at 99 m shown in (b) demonstrates that the thermocouple responds faster and measures more variance at shorter spatial scales than the thermistor.

b. Frequency response

In the time domain, the thermocouple's response appears notably faster than the thermistors', especially at the faster profiling speed, 1.2 m s^{-1}. Two progressively expanded excerpts from Fig. 4 are shown in Fig. 5. At large scales, the thermocouple measures the same profile as the thermistor, while at smaller scales, the thermocouple captures much more variability, as evident from the turbulent patch between 98.8 and 100.2 m (Fig. 5b).

At slower speeds, (0.32 m s^{-1}; Fig. 6), the difference between thermocouple and thermistor is less obvious because the thermistor resolves a greater fraction of the variability. On large scales, both sensors are clearly measuring similar temperature structure. One must look to the temperature-gradient spectra to quantify the high-frequency response.

We compare the frequency response of thermocouple and thermistor using the microconductivity probe as a benchmark. At a 1.2 m s^{-1} fall speed, the 3-dB point of the microconductivity probe is 360 Hz (=300 cpm $\times$ 1.2 m s^{-1}), which is much higher than the thermocouple channel's 204.8-Hz Nyquist frequency. Figure 7 shows $\Psi_{T_z}/\Psi_{\mu C_z}$, the ratio of the power spectrum of temperature gradient (measured by both thermocouple and thermistor) to the power spectrum of conductivity gradient, calibrated using Eq. (2).

Bin-averaged spectra were used to calculate $\Psi_{T_z}/\Psi_{\mu C_z}$, each with 10 degrees of freedom. For each of the 104 turbulent patches (73 patches at $\sim$1.2 m s^{-1} and 31 patches at $\sim$0.3 m s^{-1}) this ratio was further averaged

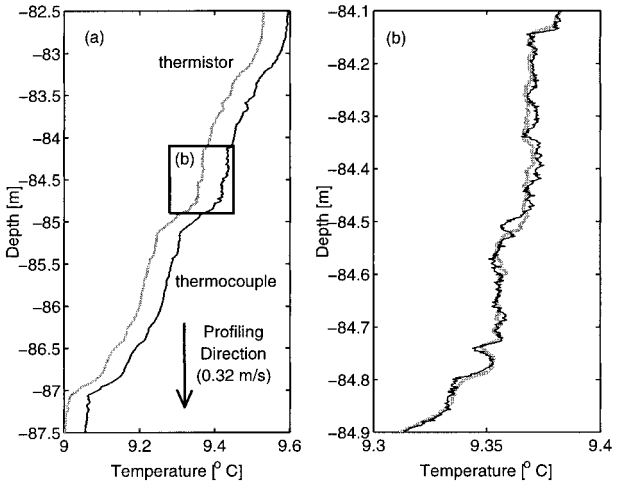

FIG. 6. As in Fig. 5 except profiling downward at 0.32 m s^{-1}. The expanded view (b) of the patch at 84.5 m demonstrates that the spatial response of the thermocouple and thermistor are more similar at this slow profiling speed.

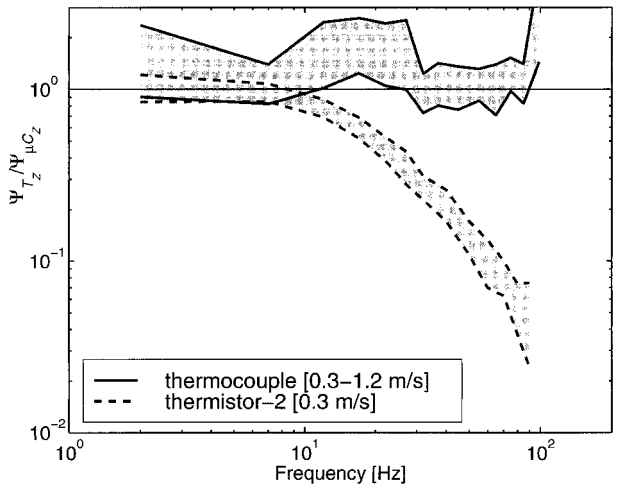

FIG. 7. Spectral power of the thermocouple and thermistor temperature gradient normalized by temperature gradient inferred from the microconductivity probe. The shaded regions represent 95% bootstrap confidence limits.

into 20 bins and 95% bootstrap confidence intervals calculated. Only patches with small salinity gradient were used. Profiling speed did not significantly affect the thermocouple response, so that the thermocouple transfer function represents patches from both 0.3 and 1.2 m s^{-1}, while the response for the thermistor was found to depend on both profiling speed and the unique characteristics of each thermistor. These effects are discussed in the appendix.

The transfer function $\Psi_{T_z}/\Psi_{\mu C_z}$ of the thermocouple is near unity in the frequency band 0–100 Hz. We have not been able to determine an upper bound on the thermocouple's frequency response, except that it exceeds 100 Hz. The departure from 1 near 20 Hz may result from salinity contamination of $\Psi_{\mu C_z}$. Since 80% of the spectra are from regions where $dT/dS < 0$, the (temperature–salinity) *T*–*S* gradient cross spectrum $\Psi_{S_zT_z}$ partially negates the temperature-gradient contribution to the conductivity-gradient spectrum near $k_b/10 < k < k_b/2$ if *T* and *S* are significantly correlated (Washburn et al. 1996; Nash and Moum 1998). As a result, the ratio $\Psi_{T_z}/\Psi_{\mu C_z}$ is slightly enhanced at these wavenumbers (which correspond to ~20 Hz).

c. Noise

To determine noise levels, spectra were taken from the quietest regions of a cast (Fig. 8). In this figure, the raw thermistor noise and the thermistor noise after correcting for the probe's frequency response (i.e., applying the inverse of the response in Fig. 7 to the noise spectrum) are shown. The noise in the frequency-corrected thermistor's signal is found to be less than the thermocouple's at frequencies below 100 Hz. Dimensionalized theoretical spectra (Batchelor 1959) with χ_T calculated from the thermocouple-gradient spectrum and ϵ determined from shear probes are shown for comparison.

The noise in the undifferentiated thermocouple signal is found to be white at a mean level of $\sim 4 \times 10^{-9}$ K^2 Hz^{-1}, which corresponds to an rms noise of 0.6 mK in the 10–100-Hz frequency band. This is consistent with the noise spectrum for the differentiated signal shown in Fig. 8 and is much noisier than that achieved by thermistors. For example, Gregg et al. (1978) achieved a thermistor noise level of 3-μK rms in the 10–100-Hz band.

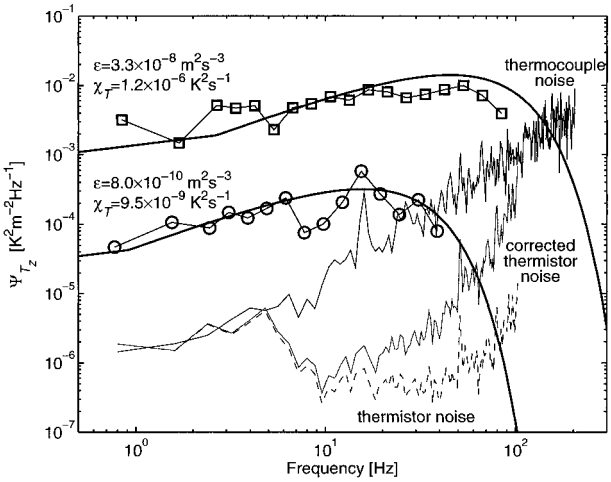

FIG. 8. Temperature-gradient spectra as measured with the thermocouple for two turbulent patches with different ϵ and χ_T while profiling at 1.2 m s^{-1}. Here ϵ was determined from shear probe measurements on Chameleon. The dark lines represent the appropriate Batchelor spectra with $q = 3.7$. A typical thermocouple noise spectrum is shown in black. The dashed line represents a typical thermistor noise spectrum. The gray line shows this same noise after applying the correction for the thermistor's limited frequency response.

The thermocouple noise can be completely accounted for by considering the input noise at the first amplifier (AD745). The rms input noise (from Analog Devices' specifications) is 5.5 nV/$\sqrt{\text{Hz}}$ at 10 Hz and 3.6 nV/$\sqrt{\text{Hz}}$ at 100 Hz. Hence, about 45 nV of rms noise can be expected at the input over the 10–100-Hz bandwidth. After amplification, this corresponds to a 0.37-mV rms noise, which calibrates to a 0.75-mK rms, a value slightly larger than measured.

4. Gradient spectra

To estimate χ_T from unresolved temperature measurements (such as those by thermistor sensors from high-speed profilers), a universal scalar gradient spectrum must be assumed to describe the high-wavenumber behavior. The shape and universality of such a spectrum are in question. Nevertheless, temperature-gradient spectra measured in the ocean have usually tended toward the Batchelor (1959) form with $q = 3.7$ (Oakey 1982; Caldwell et al. 1980); such spectra with nondimensionalization for spectral amplitude $\Psi_{T_z} k_b D_{T\chi T}^{-1}$and wavenumber k/k_b are used for comparison here.

A comparison of nondimensional scalar spectra for the thermocouple, thermistor, and theory is shown in Fig. 9 for profiles made at 1.2 m s^{-1}. Turbulent patches have been separated into four different ranges of ϵ and bin-averaged to illustrate that the fraction of variance captured by the thermistor probe depends on ϵ. This is because scalar fluctuations extend to higher wavenumbers in more energetic turbulence. The thermistor measures 12% of the temperature gradient variance for patches with $\langle\epsilon\rangle = 2.1 \times 10^{-9}$ m^2 s^{-3} (Fig. 9a), but only 4% of the variance for patches with $\langle\epsilon\rangle = 1.1 \times 10^{-7}$ m^2 s^{-3} (Fig. 9d). In contrast, the thermocouple appears to resolve the entire temperature-gradient spectrum at these turbulent intensities.

Averaged nondimensional spectra were also computed for turbulent patches observed while profiling at 0.3 m s^{-1} (Fig. 10). Much more energetic patches [$\langle\epsilon\rangle = 3.3 \times 10^{-6}$] can be resolved by the thermocouple at this speed. However, the thermistor still needs substantial correction at high wavenumbers.

5. Range of applicability

Whether a thermocouple or thermistor is more appropriate depends on the relative intensities of temperature-gradient fluctuations and velocity fluctuations. Figure 11 shows the theoretical temperature-gradient spectrum for three values of χ_T and ϵ relative to the thermocouple noise spectrum. For $\chi_T \sim 10^{-7}$ K^2 s^{-1}, the thermocouple fully resolves Ψ_{T_z} at low dissipation rates and mostly resolves Ψ_{T_z} at higher rates ($\epsilon \sim 10^{-8}$ m^2 s^{-3}). When the temperature microstructure is much weaker ($\chi_T \sim 10^{-7}$ K^2 s^{-1}) and the dissipation rate is large, the theoretical Ψ_{T_z} is beneath the noise and thus not resolved by the thermocouple.

The usefulness of the thermocouple relative to the thermistor can be quantified by comparing the fraction of Ψ_{T_z} resolved by each sensor as a function of both ϵ and χ_T (Fig. 12).

6. Summary

The fast response time of the thermocouple makes it suitable for measuring a temperature gradient from a rapidly moving profiler. Because corrections for the thermocouple response are not required, it is suitable for investigating the spectral shape of temperature gradient at high wavenumbers. It is robust and not sensitive to fouling or corrosion. However, because its signal is small, amplifier noise currently limits its usefulness to measuring turbulent patches with a relatively large temperature-gradient signal, as shown in Fig. 12.

Acknowledgments. This work was supported by the Office of Naval Research (Grant N00014-96-1-0256).

APPENDIX

Thermistor Transfer Functions

Two functional forms have been suggested for the power-response transfer functions of thermistors; a single-pole filter H^2_{sp} (Lueck et al. 1977),

$$H^2_{\text{sp}}(f) = \frac{1}{1 + (f/f_c)^2}, \tag{A1}$$

and a double-pole filter H^2_{dp} (Gregg and Meagher 1980),

$$H^2_{\text{dp}}(f) = \left(\frac{1}{1 + (f/f_c)^2}\right)^2. \tag{A2}$$

The cutoff frequency of the filter, f_c, represents the 3-dB point for $H^2_{\text{sp}}(f)$ [Eq. (A1)], but is the 6-dB point for the double pole $H^2_{\text{dp}}(f)$ [eq. (A2)].

a. Dependence on profiling speed U

A number of scalings of the form $f_c = aU^b$ have been proposed to describe the transfer function's dependence on U. For a double-pole response, Gregg (1997) suggests

$$\tau = 0.005U^{-0.32} \quad \text{and} \quad f_c = 32U^{0.32}, \tag{A3}$$

with $\tau \equiv (2\pi f_c)^{-1}$ in seconds, f_c in hertz, and U in meters per second. These coefficients were derived from measurements made at $U = 0.08$–4 m s^{-1}. For our profiling speeds, this scaling gives $f_c = 21.2$ Hz for $U = 0.3$ m s^{-1} and $f_c = 33.7$ Hz for $U = 1.2$ m s^{-1}.

A comparison of the averaged frequency response ($\Psi_{T_z}/\Psi_{\mu C_z}$) of thermistor 2 at two profiler speeds ($U = 0.3$ and 1.2 m s^{-1}) is shown in Fig. A1. Also plotted are single- and double-pole filter response functions,

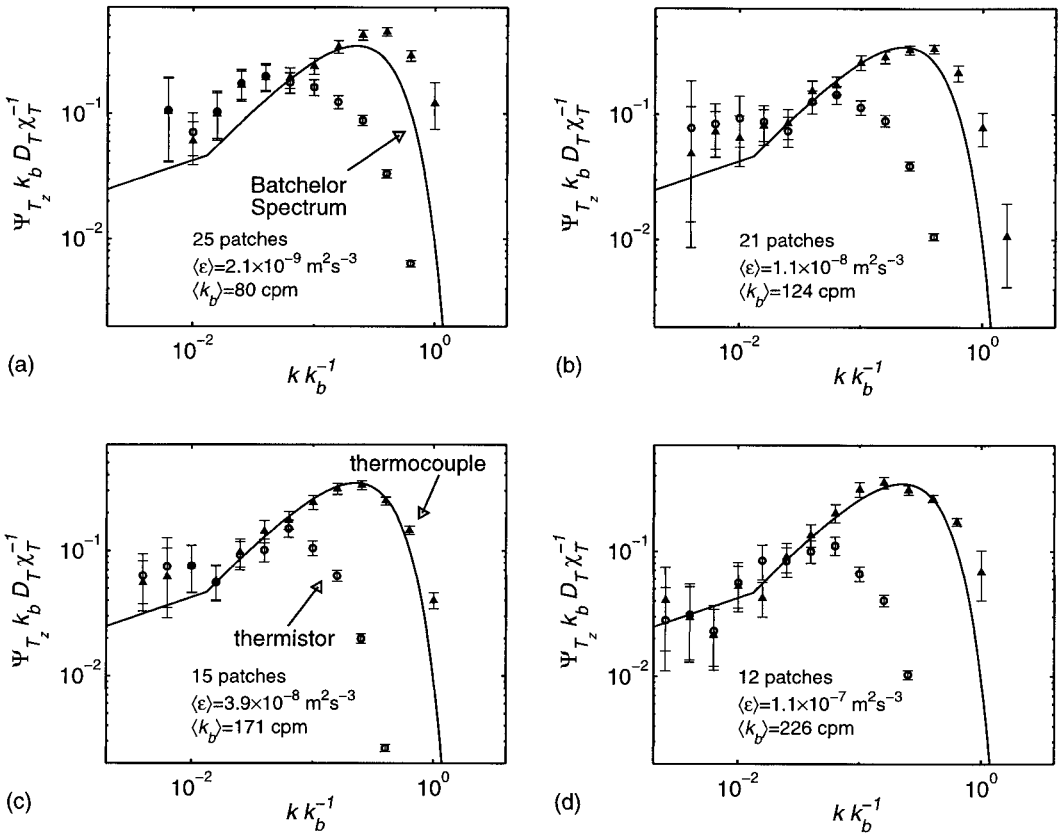

FIG. 9. Mean nondimensional temperature gradient spectra $\Psi_{T_z} k_b D_T \chi_T^{-1}$ for four different ranges of ϵ defined by Batchelor wavenumber (in cpm): (a) $k_b < 100$, (b) $100 < k_b < 150$, (c) $150 < k_b < 200$, and (d) $k_b > 200$. Spectral estimates from thermistor measurements are represented by open circles; triangles represent those from the thermocouple. Error bars represent 95% bootstrap confidence limits. Profiles were made at 1.2 m s^{-1} and no corrections for frequency response have been applied. The solid lines represent Batchelor spectra with $q = 3.7$ calculated for the mean ϵ and χ_T of the included patches.

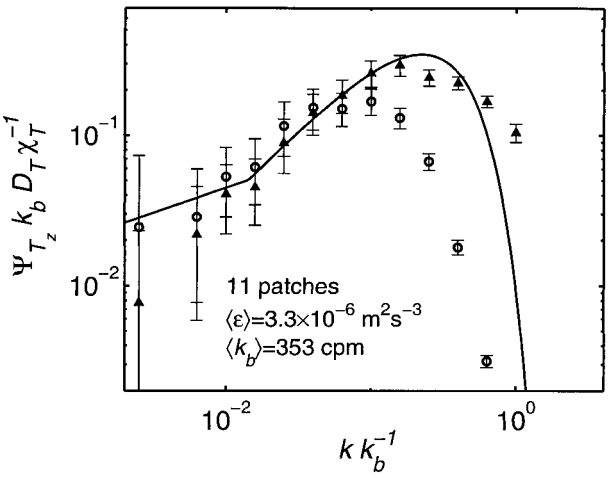

FIG. 10. As in Fig. 9 except for patches observed while profiling at 0.3 m s^{-1}. Only patches with $k_b > 200$ cpm are shown.

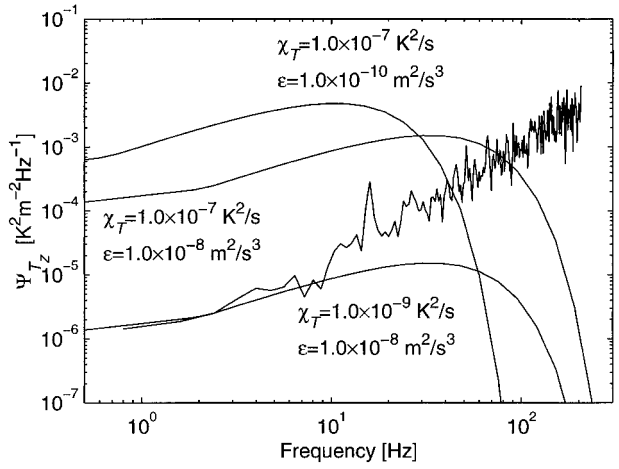

FIG. 11. Theoretical spectra of temperature gradient (Batchelor 1959) for a range of χ_T and ϵ relative to the thermocouple noise (1.2 m s^{-1} profiling speed).

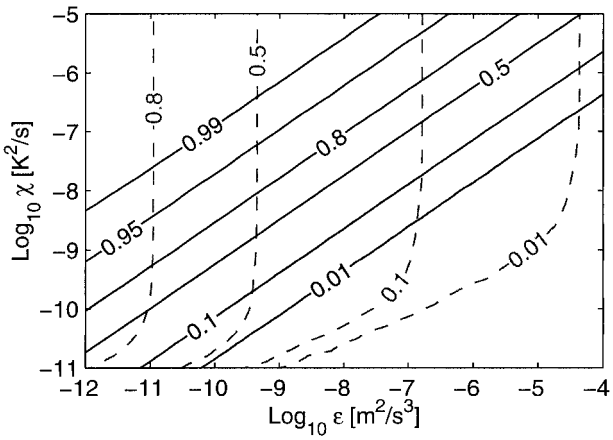

FIG. 12. Fraction of variance resolved by the thermocouple (solid line) and thermistor (gray dashed line) as a function of ϵ and χ_T for a 1.2 m s^{-1} profiling speed. For the thermocouple, the resolved variance is limited by the intersection of the Batchelor spectrum with the noise spectrum (from Fig. 11). In contrast, the thermistor is limited by its frequency response (~single pole, f_c = 20 Hz, see the appendix) except when ϵ is large and χ_T is low. The shaded area represents the region where the thermistor measures more variance of the temperature-gradient spectrum than the thermocouple. The unshaded area represents the region where the thermocouple measures more variance than the thermistor.

which have been fitted to the data[4] over the frequency range from 0 to 50 Hz. For this sensor, we find that $f_c \sim U^{0.123}$. Thermistor 1 (not plotted) gives a similar dependence $f_c \sim U^{0.120}$. We conclude that these probes show a much weaker dependence on profiling speed than Eq. (A3). Further, it is not clear which frequency response function (single- or double-pole) best models the thermistor's response.

b. Sensor individuality

Less well documented is the fact that the cutoff frequency and the shape of the frequency response depend on the individual thermistor used. Figure A2 shows the ratio $\Psi_{T_z}/\Psi_{\mu C_z}$ for each of two thermistors, averaged over 31 turbulent patches while profiling at 0.3 m s^{-1}. From the figure, it is clear that there are significant differences in frequency response between the two. Not only are the two probes best described by transfer functions with different f_c, but thermistor 1 is described better by a double-pole filter response, while thermistor 2 is much closer to a single pole. These sensor-to-sensor variations are much more significant than the effects of profiling speed.

[4] In each case, f_c was determined by minimizing the residual least squares logarithmic error between data and filter transfer function, i.e., minimization of $\int_{f=0\ \mathrm{Hz}}^{50\ \mathrm{Hz}} [\log(\Psi_{T_z}(f)/\Psi_{\mu C_z}(f)] - \log[H^2(f)]\ df$.

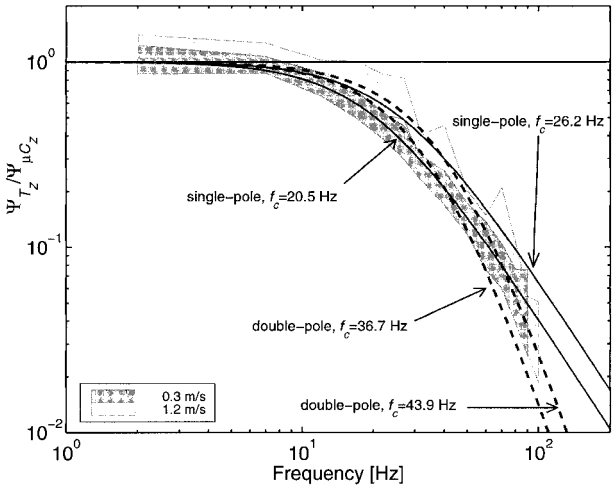

FIG. A1. The frequency response ($\Psi_{T_z}/\Psi_{\mu C_z}$) for a single thermistor at two different profiling speeds. Each shaded region represents the 95% bootstrap confidence interval for the average over tens of turbulent patches: the dark shaded region represents 73 patches with U = 1.2 m s^{-1}; the light region represents 31 patches with U = 0.3 m s^{-1}. Smooth curves represent best-fits of the response to a single- or double-pole filter transfer function.

c. Applying frequency corrections

To illustrate the errors that may be introduced by applying spectral corrections, we apply single- and double-pole corrections to our observed $\Psi_{T_z}/\Psi_{\mu C_z}$. Figure A3 shows the effects of choice of the assumed response function and f_c on the transfer function of our thermistors. In Fig. A3a we applied a single-pole filter correction to the data, with f_c fit to the data between 0 and 50 Hz. In Fig. A3b we applied a double-pole filter cor-

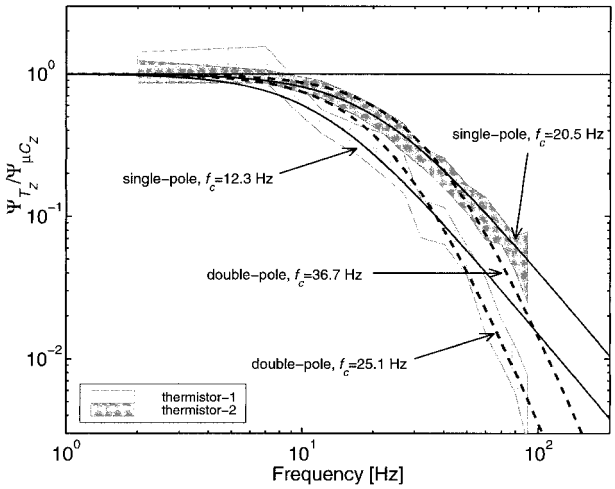

FIG. A2. The frequency response ($\Psi_{T_z}/\Psi_{\mu C_z}$) for two different thermistors while profiling at 0.3 m s^{-1}. Each shaded region represents the 95% bootstrap confidence interval for an individual thermistor (thermistor 1 is lightly shaded, thermistor 2 is dark). Averages for each thermistor were made over the same 31 turbulent patches. Each smooth curve represents a best-fit of the response to a single- or double-pole filter transfer function.

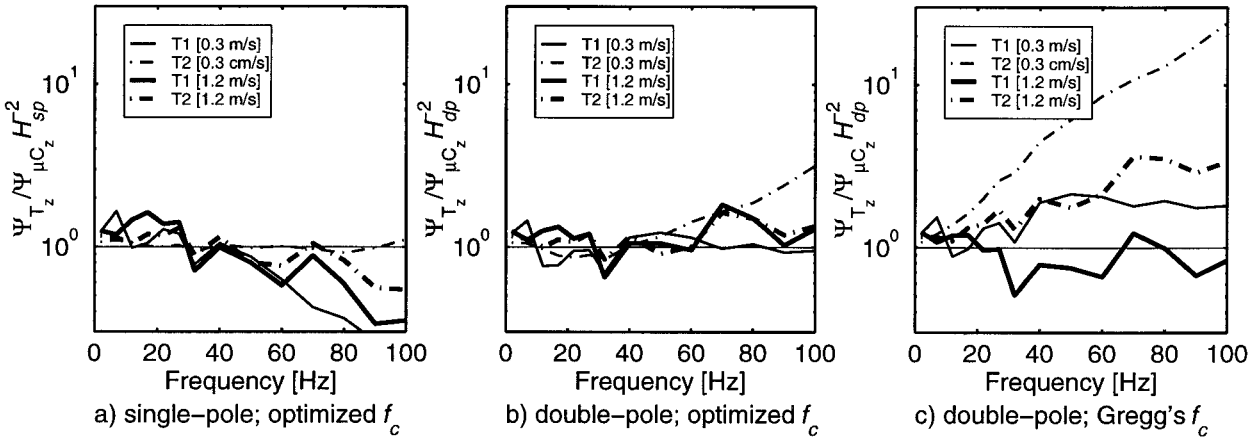

FIG. A3. Thermistor response corrected using a single- or double-pole filter as a model for the thermistor frequency response. In (a) and (b), f_c was chosen to fit the data between 0–50 Hz; in (c) Eq. (A3) was used to estimate f_c.

rection to the data, with f_c fit to the data between 0 and 50 Hz. In Fig. A3c we applied the double-pole correction (Gregg 1997) with f_c determined from Eq. (A3).

For optimized f_c, single-pole corrections (Fig. A3a) are conservative and may underpredict the response by a factor of 2–3 (note that thermistor 2 at 0.3 m s^{-1} is well described by this single-pole correction). However, double-pole corrections (Fig. A3b) tend to overpredict the response by a factor of 2–3, although T1 at 0.3 m s^{-1} is very well described by the double-pole response.

Generally it is not possible to determine f_c individually, so that Eq. (A3) must be used, as shown in Fig. A3c. Using this equation, spectral values may be overpredicted by as much as a factor of 20.

From these examples, it is clear that a universal transfer function *may* be able to include some of the effects of profiling velocity but cannot account for thermistor individuality, an effect we find to be much more important. Hence, if thermistors are to be used to determine dT/dz at frequencies above ~20 Hz, it is first necessary to determine the transfer function of the thermistor experimentally before applying a frequency correction.

REFERENCES

Balko, B., and R. L. Berger, 1968: Measurement and computation of thermojunction response times in submillisecond range. *Rev. Sci. Instrum.,* **39,** 498–503.

Batchelor, G. K., 1959: Small-scale variation of convected quantities like temperature in turbulent fluid. *J. Fluid Mech.,* **5,** 113–133.

Beckman, P., R. P. Roy, K. Whitfield, and A. Hasan, 1993: A fast-response microthermocouple. *Rev. Sci. Instrum.,* **63,** 2947–2951.

Caldwell, D. R., T. M. Dillon, J. M. Brubaker, P. A. Newberger, and C. A. Paulson, 1980: The scaling of vertical temperature gradient spectra. *J. Geophys. Res.,* **85,** 1917–1924.

Fish, G., O. Bouevitch, S. Kokotov, K. Lieberman, D. Palanker, I. Turovets, and A. Lewis, 1995: Ultrafast response micropipette-based submicrometer thermocouple. *Rev. Sci. Instrum.,* **66,** 3300–3306.

Gargett, A. E., 1985: Evolution of scalar spectra with the decay of turbulence in a stratified fluid. *J. Fluid Mech.,* **159,** 379–407.

Gregg, M. C., 1997: Uncertainties and limitations in measuring ϵ and χ_T. *Microstructure Sensors in the Ocean, a Workshop,* Mt. Hood, OR, Office of Naval Research, 98–108.

——, and T. B. Meagher, 1980: The dynamic response of glass-rod thermistors. *J. Geophys. Res.,* **85,** 2779–2786.

——, ——, A. Pederson, and E. Aagaard, 1978: Low noise temperature microstructure measurements with thermistors. *Deep-Sea Res.,* **25,** 843–856.

Head, M. J., 1983: The use of miniature four-electrode conductivity probes for high resolution measurement of turbulent density or temperature variations in salt-stratified water flows. Ph.D. thesis, University of California, San Diego, 211 pp.

Kraichnan, R., 1968: Small-scale strucutre of a scalar field convected by turbulence. *Phys. Fluids,* **11,** 945.

Lieberman, L., 1951: The effect of temperature inhomogeneities in the ocean on the propagation of sound. *J. Acoust. Soc. Amer.,* **23,** 563–570.

Lueck, R. G., O. Hertzman, and T. R. Osborn, 1977: The spectral response of thermistors. *Deep-Sea Res.,* **24,** 951–970.

Marmorino, G. O., and D. R. Caldwell, 1978: Horizontal variation of vertical temperature gradients measured by thermocouple arrays. *Deep-Sea Res.,* **25,** 221–230.

Moum, J. N., M. C. Gregg, R. C. Lien, and M. E. Carr, 1995: Comparison of turbulence kinetic energy dissipation rate estimates from two ocean microstructure profilers. *J. Atmos. Oceanic Technol.,* **12,** 346–366.

Nash, J. D., and J. N. Moum, 1999: Estimating salinity variance dissipation rate from conductivity microstructure measurements. *J. Atmos. Oceanic Technol.,* **16,** 263–274.

Oakey, N. S., 1982: Determination of the rate of dissipation of turbulent energy from simultaneous temperature and velocity shear microstructure measurements. *J. Phys. Oceanogr.,* **12,** 256–271.

Omega Engineering, 1995: *The Temperature Handbook.* Omega Engineering. [Available online at www.omega.com.]

Osborn, T. R., and C. S. Cox, 1972: Oceanic fine structure. *Geophys. Fluid Dyn.,* **3,** 321–345.

Urick, R. J., and C. W. Searfoss, 1948: The microthermal structure of the ocean near Key West, Florida. Tech. Rep. S-3392, Naval Research Laboratory, 26 pp.

Washburn, L., T. F. Duda, and D. C. Jacobs, 1996: Interpreting conductivity microstructure: Estimating the temperature variance dissipation rate. *J. Atmos. Oceanic Technol.,* **13,** 1166–1188.